**Proceedings of the 2nd Biennial IEEE/RAS-EMBS International Conference on Biomedical Robotics and Biomechatronics Scottsdale, AZ, USA, October 19-22, 2008**

# Connection Vector Fields for Underactuated Systems

Ross L. Hatton and Howie Choset
{rlhatton, choset}@cmu.edu

***Abstract*— In this paper, we build off results from geometric mechanics to gain fresh insight into the locomotion of underactuated systems. More specifically, we use the connection, which relates body velocity to internal shape changes, to create a set of vector fields on the shape space. Each of these fields corresponds to one component of the body velocity (forward, lateral, rotational), and together they highlight how a given shape change will move the system through ambient space. To demonstrate this approach, we use it to analyze the motion of several model systems, both simulated and physically instantiated.**

## I. Introduction

Locomotion is an active area of study, with a rich literature approaching the subject from both biological and controls/physics standpoints. There is much crossover between these approaches, with biological observation driving biomimetic robot development, and physical analysis providing interpretation of biological data.

In this paper, we use physical analysis to consider the locomotion problem for multibody, underactuated systems moving on smooth, level surfaces. Past work in this area has focused on identifying the *net* motion resulting from gaits (cyclic shape changes). Such approaches work well for capturing the bulk motions of these systems through open spaces, but miss the intermediate motions. These intermediate motions are especially important when planning motions that avoid obstacles while moving the system through cluttered spaces. Additionally, these methods rely on the property of gaits that they start and end in the same shape, forming a closed loop in the shape space; they thus provide no insight as to the position change resulting from shape changes that don't form a closed loop.

To more fully understand and control these systems, we wish to go further and characterize the intermediate motions, with methods that work for shape changes in general and are not limited to gaits. To this end, we use established techniques from geometric mechanics to find the *connections* for our systems, which relate shape and body velocities. We then use these relationships to form a set of vector fields on the shape space. By comparing given shape changes against these fields, we identify key characteristics of the resulting motions through ambient space. These characterizations are valuable both for designing locomotion strategies for robots and for understanding why biological strategies work.

## II. Prior Work

Our work builds on the body of locomotion literature using geometric mechanics to separate internal shape changes from the external motions they produce. The application of geometric mechanics to locomotion, pioneered by Shapere and Wilczek [1] and further developed by Murray and Sastry [2] and Kelly and Murray [3], provides a powerful mathematical framework for analyzing locomotion. A key product of this work is the development of the *reconstruction equation* for nonholonomic systems, which relates body velocity to changes in internal shape for a broad class of locomoting systems. We will not rederive the reconstruction equation here; for a thorough treatment, see [4]–[6].

Ostrowski *et al.* [5], [7] combined the reconstruction equation with Lie bracket theory to generate sinusoidal gaits which translate and rotate a variety of snake-like systems. Bullo and Lynch used the reconstruction equation to decouple the locomotion of kinodynamic systems and design kinematic gaits [8]. More recently, there has been interest in applying these techniques to swimming robots, such as McIsaac and Ostrowski's work on anguilliform (eel-like) robots [9] and Morgansen's work on fish [10], both of which combine the geometric approach with biomimetic elements.

It is not generally possible to integrate the reconstruction equation in closed form, raising difficulties for the inverse problem of finding shape changes which result in desired translations. In special cases, however, Stokes's theorem can be used to find the net resulting motion from gaits [3]. Mukherjee [11] used this principle to analyze the motion of rolling disks. Shammas *et al.* [6], [12] built on this approach to define functions on the shape space of their three-link robots, which allowed the design of gaits resulting in sign-definite displacements. A similar technique was used by Melli *et al.* [13] to generate gaits for a swimming robot.

## III. Background Material

The present work makes use of key results from geometric mechanics, the salient points of which we review here.

### A. Fiber Bundles and Connections

The configuration $q \in Q$ of a multibody, mobile robot separates naturally into $q = (g, r)$, where $g \in G$ is the position and orientation of the system in the ambient space, and $r \in M$ is the shape of the system, *i.e.*, the relative positions of the component bodies. In the parlance of differential geometry, this separation is equivlent to assigning to $Q$ the structure of a *trivial fiber bundle*, with $G$ the *fiber space* and $M$ the *base space*.

A further property of the systems we are investigating is that their dynamics are simplified through consideration in terms of body coordinates. When expressed in body

**978-1-4244-2883-0/08/$25.00 ©2008 IEEE**

coordinates, the Lagrangians, $L(q, \dot{q})$, of these systems are independent of the fiber variables, and as such can be replaced with the *reduced Lagrangian*, $l(\xi, r, \dot{r})$, where $\xi$ is the *body velocity*, the fiber velocity expressed in the instantaneous local coordinate frame of the robot. The relationship between $\dot{g}$ and $\xi$, for a robot which translates and rotates in the plane, and whose fiber space is thus $SE(2)$, is illustrated in Fig. 1. A useful interpretation of the three components of $\xi$ in $SE(2)$ is that $\xi_x$ is the longitudinal velocity, $\xi_y$ the lateral velocity, and $\xi_\theta$ the rotational velocity of the system.

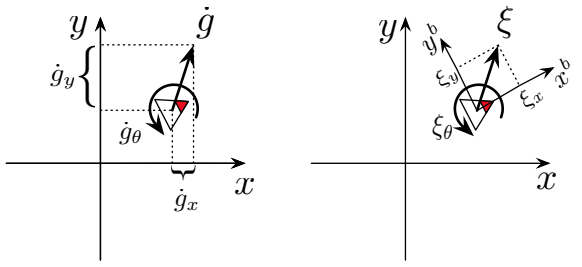


(a) Fiber velocity. (b) Body velocity.

Fig. 1. Two representations of the velocity of a robot. The robot, represented by the triangle, is translating up and to the right, while spinning counterclockwise. In (a), the *fiber velocity*, $\dot{g}$, is measured with respect to the global frame. The *body velocity*, $\xi$, in (b) is the fiber velocity represented in the robot's instantaneous local coordinate frame.

Similarly, the constraints on these systems are solely functions of the shape variables and body velocity. Together, these body representations of the robot dynamics and constraints can in turn be used to formulate a *connection* [4] on $Q$ which defines allowable combinations of body and shape velocities. Here, this lets us reduce control of the whole system to control of the robot's shape. We use the connection to build the *reconstruction equation* [4] for the system,

$$\xi = -\mathbf{A}(r)\dot{r} + \mathbf{\Gamma}(r)p, \tag{1}$$

where $\mathbf{A}(r)$ is a matrix denoting the local form of the *mixed nonholonomic connection*, $\mathbf{\Gamma}(r)$ is the *momentum distribution function*, and $p$ is the *generalized nonholonomic momentum*, which is directed along the unconstrained fiber directions of the system. [4]

For two important classes of underactuated systems, the generalized momentum drops out of the equation [6]. *Principally kinematic* systems have as many constraints as fiber degrees of freedom, and thus no generalized momentum. The equations of motion for *purely mechanical* systems are based solely on conservation of momentum, which results in $\dot{p} = 0$. When the robot starts at rest, *i.e.* $p(0) = 0$, the generalized momentum remains zero for all time. For both classes of systems, the reconstruction equation is thus further reduced to the *kinematic reconstruction equation*,

$$\xi = -\mathbf{A}(r)\dot{r}. \tag{2}$$

and the local connection thus acts as a kind of Jacobian, mapping from velocities in the base space to the corresponding body velocity. For the rest of this paper, we will limit our attention to these kinematic systems.

### B. Shape Changes

As we are interested in locomotion, *i.e.* how patterned joint motions result in position changes, we define several operations in the shape space of a robot: shape changes and gaits.

*Definition 3.1 (Shape change):* A shape change $\psi \in \Psi$ is a trajectory in the base space $M$ of the robot over an interval $I = [0, T]$, *i.e.*

$$\begin{aligned} \psi : I &\rightarrow M \\ t &\mapsto r. \end{aligned} \tag{3}$$

Having defined shape changes, we now formally define gaits.

*Definition 3.2 (Gait):* A gait $\phi \in \Phi$ is a cyclic shape change, *i.e.*

$$\Phi = \{\phi \in \Psi \mid \phi(0) = \phi(T)\}. \tag{4}$$

Note that a gait has a defined start point; two gaits whose images in $M$ are the same closed curve, but with different start points, are distinct.

## IV. Connection Vector Fields

A key feature of the integration approaches in [6] and [13] is that for low dimensional base spaces, the Stokes's theorem integrands can be plotted as height functions on the base space. Positive, negative, or zero motions in each fiber component can then be generated by choosing gaits (closed paths on the base space) that correspondingly encircle positive, negative, or zero volume under the height functions – gait design is simplified to intuitively drawing curves on the base space.

As Stokes's theorem provides solutions for net integrals on closed paths, the height functions are only applicable to finding the bulk motions resulting from gaits. Specifically, they provide no information about either the intermediate motions, which are important when navigating a robot through obstacles, or the motion resulting from a robot transitioning between two different shapes. To address these limitations, we present here a novel design tool, the *connection vector field*.

Similarly to height functions, connection vector fields are defined on the base space of the robot and capture the relationship between shape changes and their resulting fiber motions. They facilitate intuitive design and analysis of shape changes, by indicating the fiber motion resulting from curves drawn arbitrarily on the base space. However, connection vector fields relate base and fiber motion differentially, allowing for the analysis of intermediate motions and open (non-gait) shape changes.

### A. Connection Vector Field Definition

The basic formulation of our new approach is similar to that of the height functions. As with the height functions, we consider each row of the connection matrix. Instead of invoking Stokes's theorem, however, we create *connection vector fields* $\vec{\mathbf{A}}^{\xi_i}(r)$ on $M$, where the vectors in the vector field associated with the $i$th fiber direction are the natural

duals of the covectors in the $i$th row of the negative local connection,

$$\vec{\mathbf{A}}^{\xi_i}(r) = -\mathbf{A}^i(r)^\sharp. \tag{5}$$

From the equivalence of the vector/covector product and the dot product, *i.e.*,

$$\omega v = \sum_j \omega^j v_j = \omega^\sharp \cdot v, \tag{6}$$

for a vector $v$ and a covector $\omega$, we have a new expression for the kinematic reconstruction equation in (2),

$$\xi_i = \vec{\mathbf{A}}^{\xi_i}(r) \cdot \dot{r}. \tag{7}$$

Considering the local connection as a set of vector fields with the dot product operator brings strong geometric intuition to the problem of designing shape changes. The geometric interpretation of the dot product in (7) is

$$\xi_i = \vec{\mathbf{A}}^{\xi_i}(r) \cdot \dot{r} = \|\vec{\mathbf{A}}^{\xi_i}(r)\|\|\dot{r}\| \cos\Theta, \tag{8}$$

where $\Theta$ is the angle between the vectors. Taking the $\cos\Theta$ term as a measure of the alignment of $\vec{\mathbf{A}}^{\xi_i}(r)$ and $\dot{r}$, $\xi_i$ is positive, negative, or zero when the two vectors have correspondingly positive, negative, or zero alignment, and is scaled by the magnitudes of $\vec{\mathbf{A}}^{\xi_i}$ and $\dot{r}$.

By plotting a shape change $\psi$ together with each of the $\vec{\mathbf{A}}^{\xi_i}(r)$ fields, we can thus easily observe the resulting fiber motion in body coordinates, by observing $\Theta$ and $\|\vec{\mathbf{A}}^{\xi_i}\|$ along $\psi$. Note that we are intentionally disregarding $\|\dot{r}\|$ in this observation. While $\|\xi\|$ scales with $\|\dot{r}\|$, the duration of $\psi$ is inversely proportional to the latter term, which thus drops out when considering displacements, as we expect for a kinematic system.

### *B. Floating snake robot*

As a first example of the connection vector field principle, we take the three-link floating planar snake, shown in Fig. 2. It has three links which move in the plane, unconstrained except by their joints. Taking $g$ for the system as the position of the center of mass and the orientation of the middle link, and $r$ as the joint angles $\alpha_1$ and $\alpha_2$, the reconstruction equation for the snake, normalized for link length, is

$$\xi = \begin{bmatrix}\xi_x \\ \xi_y \\ \xi_\theta\end{bmatrix} = -\frac{1}{D}\begin{bmatrix}0 & 0 \\ 0 & 0 \\ a_{31} & a_{32}\end{bmatrix}\begin{bmatrix}\dot{\alpha}_1 \\ \dot{\alpha}_2\end{bmatrix}, \tag{9}$$

where

$$\begin{aligned} a_{31} &= 5 + 3\cos(\alpha_2) + \cos(\alpha_1 - \alpha_2) \\ a_{32} &= 5 + 3\cos(\alpha_1) + \cos(\alpha_1 - \alpha_2) \\ D &= 19 + 6(\cos(\alpha_1) + \cos(\alpha_2)) + 2\cos(\alpha_1 - \alpha_2). \end{aligned}$$

The presence of two zero rows in (9) reflects the use of the center of mass of the floating snake to represent its position; by conservation of momentum, the center of mass, having started at rest, cannot acquire a nonzero velocity. The robot can, however, rotate so long as its net angular momentum is zero; the third row of the local connection is thus non-zero.

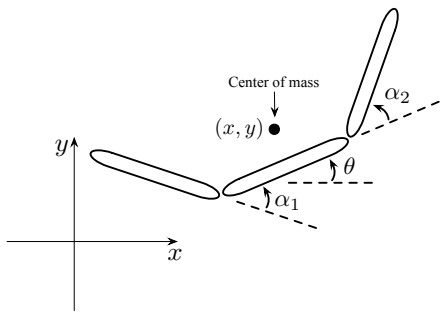


Fig. 2. Model for a floating snake. The fiber coordinates are the $x, y$ position of the center of mass and the orientation $\theta$ of the middle link with respect to the $x$ axis of the fixed coordinate system. The shape coordinates are $\alpha_1$ and $\alpha_2$, the angles of the two joints.

Eliminating the zero rows from (9) and applying (7) reduces this reconstruction equation to

$$\xi_\theta = \vec{\mathbf{A}}^{\xi_\theta}(\alpha_1, \alpha_2) \cdot \begin{bmatrix}\dot{\alpha}_1 \\ \dot{\alpha}_2\end{bmatrix}, \tag{10}$$

where

$$\vec{\mathbf{A}}^{\xi_\theta}(\alpha_1, \alpha_2) = -\frac{1}{D}\begin{bmatrix}a_{31} & a_{32}\end{bmatrix}^T. \tag{11}$$

We plot $\vec{\mathbf{A}}^{\xi_\theta}$ along with a sample gait $\phi$ in Fig. 3(a), where $\phi = \begin{bmatrix}\alpha_1 & \alpha_2\end{bmatrix}^T$ has

$$\alpha_1(t) = \frac{\pi}{4}\big(-1 + 2\cos(t + .19) + \sin(t + .19)\big) \tag{12}$$

$$\alpha_2(t) = \frac{\pi}{4}\big(\quad 1 + 2\cos(t + .19) - \sin(t + .19)\big). \tag{13}$$

The shape velocity $\dot{\phi} = \begin{bmatrix}\dot{\alpha}_1 & \dot{\alpha}_2\end{bmatrix}^T$ at time $t$ is a tangent vector to $\phi$ at $\phi(t)$. It is clear that $\dot{\phi}(t)$ has positive alignment with $\vec{\mathbf{A}}^{\xi_\theta}(\phi(t))$ over the first segment of the gait and negative alignment over the second segment, with zero alignment at the start, end, and transition between segments; we can thus immediately conclude that the robot rotates first positively, then negatively while executing the gait, as seen in Fig. 3(b).

Closer observation of Figure 3(a) reveals that $\vec{\mathbf{A}}^{\xi_\theta}$ for the floating snake has approximately constant magnitude and that its curvature results in the negatively aligned segment 2 being longer than the positively aligned segment 1. This property results in a net negative rotation for the gait, and is closely related to the results in [6], whose height functions correspond to the curl of the connection vector fields.

### *C. Differential drive car*

The floating snake is a special case, as it has only one non-zero connection vector field. Most systems will have multiple connection vector fields, which must be considered simultaneously. To illustrate this process, we examine the connection vector fields for a differential drive car. While the differential drive has relatively simple kinematics and has been extensively studied through conventional means, this simplicity allows us to highlight key aspects of our approach.

Normalized for wheel radius and body width, the reconstruction equation for the differential drive car shown in

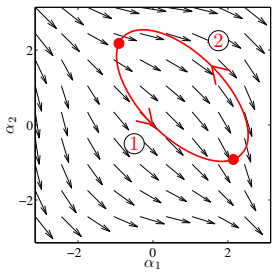


(a) $\vec{\mathbf{A}}^{\xi_\theta}$ for the floating snake, along with a sample gait $\phi$.

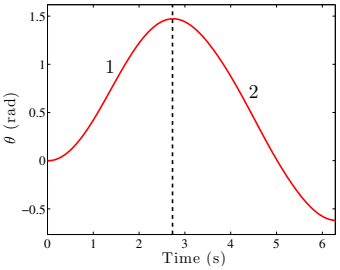


(b) Orientation $\theta$ of the snake while executing $\phi$.

Fig. 3. Sample gait $\phi$ for the floating snake. In the first segment, the shape velocity $\dot{\phi}$ is positively aligned with $\vec{\mathbf{A}}^{\xi_\theta}$, so the snake rotates positively. In the second segment, the $\dot{\phi}$ is negatively aligned with the connection vector field, resulting in negative rotation.

Fig. 4 is

$$\xi = -\begin{bmatrix} -1 & -1 \\ 0 & 0 \\ 1 & -1 \end{bmatrix} \begin{bmatrix} \dot{\alpha}_1 \\ \dot{\alpha}_2 \end{bmatrix}. \tag{14}$$

The two nonzero connection vector fields are thus

$$\vec{\mathbf{A}}^{\xi_x}(\alpha_1, \alpha_2) = \begin{bmatrix} 1 & 1 \end{bmatrix}^T \tag{15}$$

and

$$\vec{\mathbf{A}}^{\xi_\theta}(\alpha_1, \alpha_2) = \begin{bmatrix} -1 & 1 \end{bmatrix}^T. \tag{16}$$

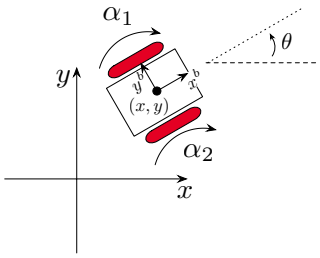


Fig. 4. Model for a differential drive car. The fiber coordinates are the $x, y$ position of the center of mass and the orientation $\theta$ with respect to the $x$ axis of the fixed coordinate system. The shape coordinates are $\alpha_1$ and $\alpha_2$, the angles of the two wheels.

The shape change $\psi$ in Fig. 5 is divided into three stages. In the first stage, $\dot{\psi}$ is aligned with $\vec{\mathbf{A}}^{\xi_x}$ and orthogonal to $\vec{\mathbf{A}}^{\xi_\theta}$. The resulting motion in the fiber space is that the robot drives forwards. In the second stage, $\dot{\psi}$ is aligned with $\vec{\mathbf{A}}^{\xi_\theta}$ and perpendicular to $\vec{\mathbf{A}}^{\xi_x}$; the robot correspondingly rotates in place. In the third and final stage, $\dot{\psi}$ has positive alignment with $\vec{\mathbf{A}}^{\xi_\theta}$ and negative alignment with $\vec{\mathbf{A}}^{\xi_x}$, leading to the robot turning while reversing.

### D. Kinematic snake

Finally, we consider the kinematic snake [6]. This system has both the richly shape-variant kinematics of the floating snake and the multiple connection vector fields of the differential drive car. The shape-variance makes the locomotion of the kinematic snake far less intuitive than that of the car, so

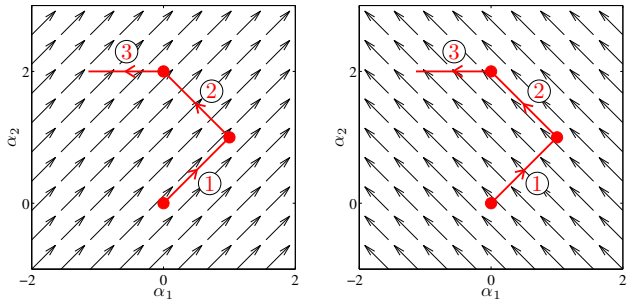


(a) $\vec{\mathbf{A}}^{\xi_x}$ (left) and $\vec{\mathbf{A}}^{\xi_\theta}$ (right) for the differential drive, along with a sample shape change $\psi$.

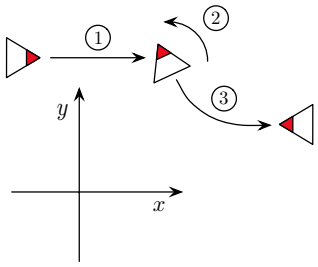


(b) Fiber motion for the differential drive resulting from $\psi$.

Fig. 5. A shape change for a differential drive car, with the effect that the robot drives forward, turns clockwise in place, and continues to turn clockwise while reversing.

our connection vector fields can provide true, novel insight for motion planning for these systems.

The three link kinematic snake is shown in Fig. 6. We take the $x, y$ position and orientation $\theta$ of the middle link of the robot as its fiber position, and the joint angles $\alpha_1$ and $\alpha_2$ as the shape. A passive wheelset on each link prevents lateral motion while allowing longitudinal and rotational motion. Normalized for link length, the reconstruction equation for the kinematic snake is

$$\xi = -\frac{1}{D}\begin{bmatrix} 1+\cos(\alpha_2) & 1+\cos(\alpha_1) \\ 0 & 0 \\ -\sin(\alpha_2) & -\sin(\alpha_1) \end{bmatrix} \begin{bmatrix} \dot{\alpha}_1 \\ \dot{\alpha}_2 \end{bmatrix}, \tag{17}$$

where $D = \sin(\alpha_1) - \sin(\alpha_2) + \sin(\alpha_1 - \alpha_2)$. The two nonzero connection vector fields are thus

$$\vec{\mathbf{A}}^{\xi_x}(\alpha_1, \alpha_2) = -\frac{1}{D}\begin{bmatrix} 1+\cos(\alpha_2) & 1+\cos(\alpha_1) \end{bmatrix}^T \tag{18}$$

and

$$\vec{\mathbf{A}}^{\xi_\theta}(\alpha_1, \alpha_2) = -\frac{1}{D}\begin{bmatrix} -\sin(\alpha_2) & -\sin(\alpha_1) \end{bmatrix}^T. \tag{19}$$

These vector fields, along with two gaits taken from [6], are plotted in Fig. 7(a). Due to singularities in the vector fields at the lines $\alpha_1 = \pm\pi$, $\alpha_2 = \pm\pi$, and $\alpha_1 = \alpha_2$, we present these plots with an angle-preserving arctangent scaling on the magnitudes of the connection vector fields [6].

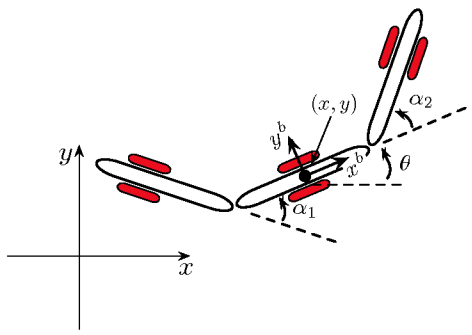


Fig. 6. Model for a kinematic snake. The fiber coordinates are the $x, y$ position and orientation $\theta$ of the middle link with respect to the fixed coordinate system. The shape coordinates are $\alpha_1$ and $\alpha_2$, the angles of the two joints. The passive wheels on each link constrain lateral but not longitudinal or rotational motion.

The two gaits are defined as

$$\phi_1 \begin{cases} \alpha_1 = -\frac{\pi}{2} + 0.637\cos(t) - 0.832\sin(t) \\ \alpha_2 = \frac{\pi}{2} + 1.013\cos(t) + 0.268\sin(t) \end{cases} \tag{20}$$

$$\phi_2 \begin{cases} \alpha_1 = -\frac{\pi}{2} + 0.637\cos(t-2.75) - 0.832\sin(t-2.75) \\ \alpha_2 = \frac{\pi}{2} + 1.013\cos(t-2.75) + 0.268\sin(t-2.75). \end{cases} \tag{21}$$

The gaits $\phi_1$ and $\phi_2$ have the same image in $M$, but, as can be seen from Fig. 7(b), result in very different fiber motions – the net effect of $\phi_1$ is to translate the snake in the $-x$ direction, while $\phi_2$ takes the robot in the $-y$ direction. This result was noted in [6], but not fully explored.

With the aid of the connection vector fields, however, we can gain additional insight into the phenomenon. In $\phi_1$, the robot starts with $\dot{\phi}_1$ negatively aligned with $\vec{\mathbf{A}}^{\xi_x}$ and orthogonal to $\vec{\mathbf{A}}^{\xi_\theta}$, and thus moves straight back. As the shape moves from state 1 to state 2, $\dot{\phi}_1$ becomes progressively antialigned with $\vec{\mathbf{A}}^{\xi_\theta}$ and orthogonal to $\vec{\mathbf{A}}^{\xi_x}$, until at 2 the fiber motion is purely negative rotation, generating a cusp in the fiber trajectory. From 2 to 3, $\dot{\phi}_1$ is positively aligned with $\vec{\mathbf{A}}^{\xi_x}$ and perpendicular to $\vec{\mathbf{A}}^{\xi_\theta}$; the robot thus moves forward until the cusp at 3 accompanies a change to backwards translation and positive rotation. As the robot reaches stage 4, the rotation fades out, leaving the robot in its original orientation, such that the backwards translation generated by the remainder of the gait is channeled into the $-x$ direction.

The second gait, $\phi_2$, contains all the same segments of motion as $\phi_1$, but in a different order. The initial configuration of $\phi_2$ is at a point of pure rotation, so the resulting fiber motion starts at what was the second cusp of $\phi_1$. Coming out of the cusp, it has rotated by $\pi/2$ radians from its original starting orientation as it starts the long translation segment from 2 to 3, sending this motion into the $-y$ fiber direction. The cusp at 4 and short translation segment serve to return the snake to its original orientation and to cancel out the accrued $x$ motion.

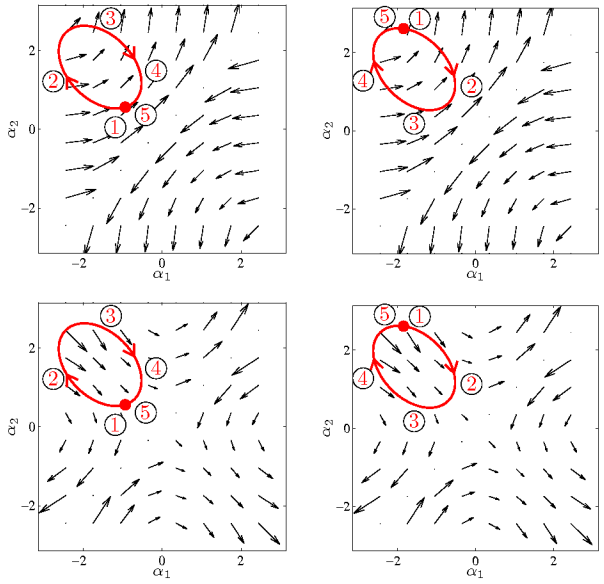


(a) Connection vector fields $\vec{\mathbf{A}}^{\xi_x}$ (top) and $\vec{\mathbf{A}}^{\xi_\theta}$ (bottom) for the kinematic snake, along with gaits $\phi_1$ (left) and $\phi_2$ (right). Note that the numbers here correspond to states, rather than sections of the gaits.

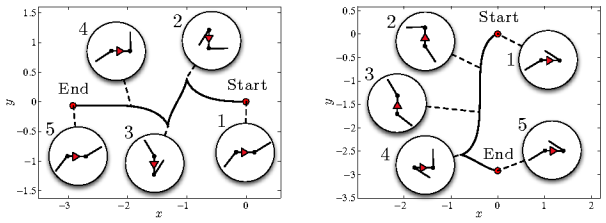


(b) Motion of the kinematic snake while executing $\phi_1$ (left) and $\phi_2$ (right). The path from "Start" to "End" is the fiber motion, and the shape of the robot at key points is shown in the insets.

Fig. 7. Two gaits for a kinematic snake.

If we consider the cusps as turning manuevers, the difference between the two gaits can roughly be characterized as $\phi_1$ having a "move-turn-turnback-move" pattern, while $\phi_2$ has a "turn-move-turnback" pattern. By shifting the balance between these two patterns, gaits can be designed to have specific net fiber motions. As these patterns can be discerned directly in the connection vector field plots of Fig. 7(a), the fields are useful evaluation tools for directing gait design.

## V. Demonstration

We built a physical instantiation of the kinematic snake, shown in Fig. 8, and instrumented it with a pair of optical computer mice to measure translation and rotation. We then implemented gaits similar to those depicted in Fig. 7 and recorded the resulting motion. For the gait shown in Fig. 9(a), which starts out with a section section aligned with $\vec{\mathbf{A}}^{\xi_x}$ and orthogonal to $\vec{\mathbf{A}}^{\xi_\theta}$, we expect the snake to translate forward, then exhibit a double cusp in its fiber motion as it changes direction twice while rotating, before traveling forward again in its original orientation. This expectation is borne out by the trace of the fiber path in Fig. 9(b). We attribute the discrepancy between the expected and actual motion of the

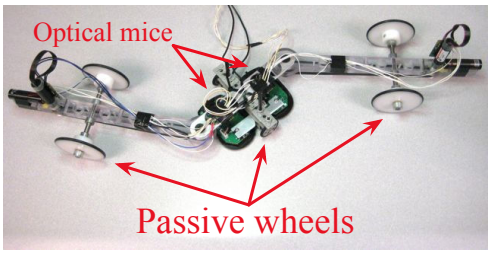


Fig. 8. Physical instantiation of the kinematic snake. Two optical mice on the middle link provide odometry data, including an estimation of constraint slip.

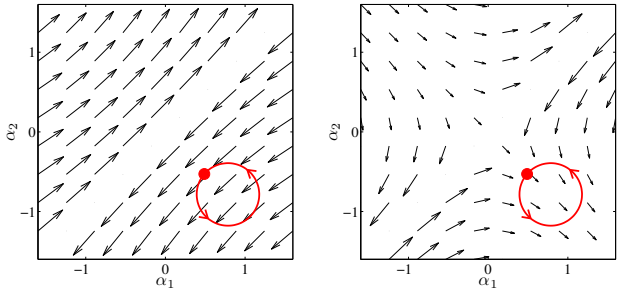


(a) Connection vector fields $\vec{\mathbf{A}}^{\xi_x}$ (left) and $\vec{\mathbf{A}}^{\xi_\theta}$ (right) for the physical kinematic snake, along with a gait.

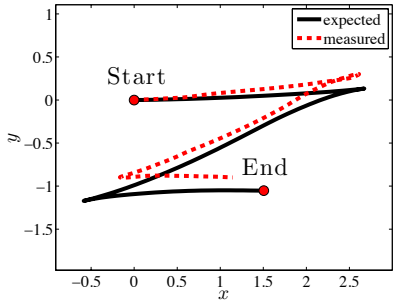


(b) Motion of the physical kinematic snake while executing the gait.

Fig. 9. Demonstration gait for the physical kinematic snake.

snake to slip in the constraining wheels, which we both observed and recorded via the optical mouse odometry.

## VI. Conclusions and Future Work

In this paper, we presented a new technique for intuitively understanding the motion of underactuated kinematic systems with symmetry. Through representing the local connections of these systems as sets of vector fields on the base space, we have been able to identify portions of shape changes as generating forward, lateral, and rotational fiber motion, without having to integrate the reconstruction equation. Further, as our approach enables at-a-glance characterization of any shape change from a single set of plots, it serves well as a design tool for generating shape changes which result in specific net and intermediate fiber motions. Unlike previous tools, the connection vector field approach works well for all shape changes, and is not limited to gaits.

Thus far, we have applied our techniques to kinematic systems with two shape variables and two nonzero connection vector fields. In our future work, we will expand our methods to work with systems with more degrees of freedom in both the base and fiber spaces, and those which have second order dynamics, such as the mixed systems of [14]. We will also seek to combine the connection vector fields with the height function methods from [6] and [13]. There is a strong opportunity for synergy between these approaches, with the height functions providing information about the net displacements from gaits while the connection vector fields deal with the intermediate motion.

## VII. Acknowledgements

We would like to thank Elie Shammas and Matthew Tesch for their input on this work.

## References

[1] A. Shapere and F. Wilczek, "Geometry of self-propulsion at low reynolds number," *Geometric Phases in Physics*, Jan 1989.

[2] R. Murray and S. Sastry, "Nonholonomic motion planning: steering using sinusoids," *IEEE Transactions on Automatic Control*, Jan 1993. [Online]. Available: http://eavr.u-strasbg.fr/~bernard/education/ensps_3a/tmp/murray.pdf

[3] S. Kelly and R. M. Murray, "Geometric phases and robotic locomotion," *J. Robotic Systems*, Jan 1995. [Online]. Available: ftp://avalon.caltech.edu/pub/murray/preprints/cds/cds94-014.ps.gz

[4] A. M. Bloch *et al.*, *Nonholonomic Mechanics and Control*. Springer, 2003.

[5] J. Ostrowski and J. Burdick, "The Mechanics and Control of Undulatory Locomotion," *International Journal of Robotics Research*, vol. 17, no. 7, pp. 683 – 701, July 1998.

[6] E. A. Shammas, H. Choset, and A. A. Rizzi, "Geometric Motion Planning Analysis for Two Classes of Underactuated Mechanical Systems," *The International Journal of Robotics Research*, vol. 26, no. 10, pp. 1043–1073, 2007. [Online]. Available: http://ijr.sagepub.com/cgi/content/abstract/26/10/1043

[7] J. Ostrowski, J. Desai, and V. Kumar, "Optimal Gait Selection for Nonholonomic Locomotion Systems," *International Journal of Robotics Research*, 2000.

[8] F. Bullo and K. M. Lynch, "Kinematic controllability for decoupled trajectory planning in underactuated mechanical systems," *IEEE Transactions on Robotics and Automation*, vol. 17, no. 4, pp. 402–412, August 2001.

[9] K. McIsaac and J. P. Ostrowski, "Motion planning for anguilliform locomotion," *Robotics and Automation*, Jan 2003. [Online]. Available: http://ieeexplore.ieee.org/xpls/abs_all.jsp?arnumber=1220714

[10] K. Morgansen, B. Triplett, and D. Klein, "Geometric methods for modeling and control of free-swimming fin-actuated underwater vehicles," *Robotics*, Jan 2007. [Online]. Available: http://ieeexplore.ieee.org/xpls/abs_all.jsp?arnumber=4399955

[11] R. Mukherjee and D. Anderson, "Nonholonomic Motion Planning Using Stokes' Theorem," in *IEEE International Conference on Robotics and Automation*, 1993.

[12] E. Shammas, K. Schmidt, and H. Choset, "Natural Gait Generation Techniques for Multi-bodied Isolated Mechanical Systems," in *IEEE International Conference on Robotics and Automation*, 2005.

[13] J. B. Melli, C. W. Rowley, and D. S. Rufat, "Motion Planning for an Articulated Body in a Perfect Planar Fluid," *SIAM Journal of Applied Dynamical Systems*, vol. 5, no. 4, pp. 650–669, November 2006.

[14] E. A. Shammas, H. Choset, and A. A. Rizzi, "Towards a Unified Approach to Motion Planning for Dynamic Underactuated Mechanical Systems with Non-holonomic Constraints," *The International Journal of Robotics Research*, vol. 26, no. 10, pp. 1075–1124, 2007. [Online]. Available: http://ijr.sagepub.com/cgi/content/abstract/26/10/1075